

# PanoLlama: Generating Endless and Coherent Panoramas with Next-Token-Prediction LLMs

Teng Zhou<sup>1</sup>, Xiaoyu Zhang<sup>1</sup>, Yongchuan Tang<sup>1\*</sup>

<sup>1</sup>College of Computer Science and Technology, Zhejiang University

## Abstract

*Panoramic Image Generation has emerged as an important task in image generation, driven by growing demands for large-scale visuals in creative and technical applications. While diffusion models have dominated this field, they face inherent limitations, including the multilevel-coherence challenge and implementation complexity, leading to suboptimal outcomes. In this paper, we introduce PanoLlama, a novel framework that redefines panoramic image generation as a next-token prediction task. Building on the pre-trained LlamaGen architecture, we generate images in an autoregressive manner and develop an expansion strategy to handle size limitations. This method aligns with the image token structure in a crop-wise and training-free manner, resulting in high-quality panoramas with minimal seams and maximum scalability. PanoLlama demonstrates its effectiveness and versatility in our experiments, achieving the best overall performance while offering flexibility for multi-scale, multi-layout, and multi-guidance generation. It overcomes the challenges that diffusion-based methods fail to address, setting a new paradigm for panoramic image generation tasks. Code is available at <https://github.com/0606zt/PanoLlama>.*

## 1. Introduction

Panoramic Image Generation (PIG) [3, 15, 38] has gained significant attention as a subtask in image generation, especially with the growing interest in visual information recording and artistic expression. A major challenge in this field is how to achieve seamless and coherent panoramas of arbitrary size.

In recent years, diffusion models [25] have become the mainstream method in image generation, proving effective in visual synthesis, restoration, and multi-modal tasks [7, 13, 22]. They employ diffusion-denoising Markov chains to map data distribution to Gaussian distribution, as demonstrated in works like DDPM [12], DDIM [26], and

LDM [21]. Diffusion-based methods for panorama generation typically operate under the joint diffusion strategy [3, 15, 19], where the large panoramic space is segmented into smaller crops, individually denoised, and then fused back into the original large one through optimization processes. While effective, these approaches face two major limitations:

1. **Multilevel-Coherence Challenge:** The objective of PIG is to achieve coherence across both low-level features (e.g., color, texture, edges) and high-level features (e.g., layout, structure, semantics), a multilevel goal that is challenging to define and balance with diffusion-based methods.
2. **Implementation Complexity:** Achieving crop-wise generation is non-trivial. These methods require complex designs to reconcile different denoising paths across image crops, which hinders both stability and scalability.

Therefore, we shifted our focus to another way of image generation, autoregressive (AR) models, which have evolved into large language models (LLMs) with stronger capabilities. AR-based approaches [2, 27, 36] introduce a tokenizer to quantize continuous image features into discrete tokens, and generate image token sequences in the way of next-token prediction.

We propose PanoLlama, a novel framework for panoramic image generation that utilizes LLMs as a scalable image generator, rather than integrating pre-trained diffusion models with optimization and fine-tuning.

1. **New Paradigm:** As illustrated in Fig. 1, we redefine PIG as a next-token prediction task, formulating panoramas as sequential data like text. It fundamentally overcomes the pending challenge in panorama generation that diffusion-based methods fail to address, achieving a SOTA performance.
2. **Speed Up:** Our framework leverages pre-trained AR models with no training, fine-tuning or tailoring, eliminating the need for time-consuming denoising iterations and optimization processes.
3. **Versatile Applications:** Beyond text-to-panorama generation, PanoLlama supports multi-scale generation for arbitrary aspect ratios, multi-layout design based on spe-

\*Corresponding Author

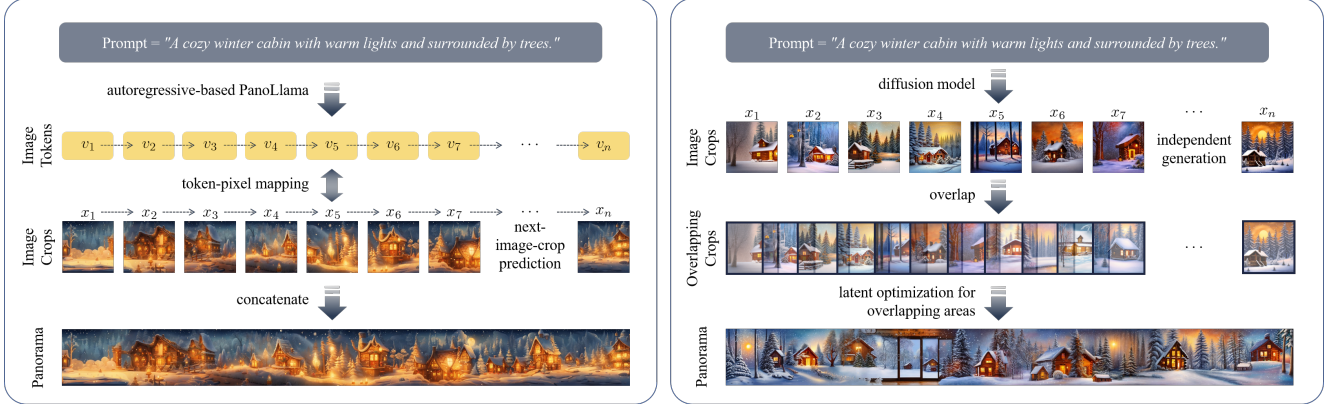


Figure 1. PanoLlama vs. diffusion-based methods in panorama generation. PanoLlama (left) is a framework that formulates PIG as a next-token prediction task. Leveraging the autoregressive properties, we build a next-crop prediction strategy that generates panoramas with high visual and semantic continuity. In contrast, diffusion-based methods (right) denoise each image crop independently and require complex optimization techniques to connect them seamlessly.

cific regions and prompts, multi-guidance generation that enables image-to-panorama synthesis.

4. **Comprehensive Evaluation:** We evaluate our method with six baselines across a range of aspects, including coherence, diversity, compatibility, efficiency, etc., ensuring the reliability of our experimental results.

## 2. Related Work

**Panorama Generation** Panorama is typically defined as images with geometric distortions for  $360^\circ$  sphere projection [16, 32, 34]. More broadly, it refers to large-scale images with coherent content, which is the focus of our discussion. Current studies mainly focus on extending pre-trained diffusion models for panorama upscaling, which can be summarized into two branches. (i) The main branch is based on the joint diffusion paradigm, splitting and merging the denoising path across different image spaces to form a larger one. This branch is pioneered by MultiDiffusion [3], which demonstrates its initial effects by taking linear interpolation to fuse different latent spaces. Building on this, many studies [15, 19, 38, 39] focus on optimizing the connection process of adjacent subareas, resulting in improved generation outcomes. (ii) Another branch utilizes image inpainting techniques to establish regional correlations for extrapolating subsequent image content [1, 14, 35]. However, as discussed in Sec. 1, diffusion-based methods often rely on specific latent optimization, which enhances the semantic smoothness but cannot guarantee pixel-level consistency, leading to suboptimal visual results.

**Autoregressive Models for Image Generation** These models introduce an image tokenizer that can apply autoregressive frameworks to generate image tokens through next-token prediction, enabling sequential modeling for vi-

sion tasks. VQVAE [31] pioneers this approach by incorporating a codebook to convert continuous image embeddings into discrete tokens; VQGAN [5, 10] further improve VQVAE by integrating adversarial and perceptual losses; PixelRNN [30] autoregressively model the dependencies between quantized pixels. With the rise of large language models, e.g., GPT [4] and Llama [29], recent studies [6, 17, 28, 33, 36] attempt to unify image generation into LLMs using an autoregressive framework, demonstrating that LLMs can be adapted to understand and generate visual content effectively. In particular, LlamaGen [27] explores the vanilla Llama architecture for scalable image generation, which yields promising results and provides valuable insights for our work.

## 3. Methodology

### 3.1. Panorama Generation as a Next-Token Prediction Task

We aim to extend a pre-trained model, originally limited to a fixed image space  $\mathcal{I} = \mathbb{R}^{H \times W \times CH}$ , to enable panorama generation over an arbitrarily large space  $\mathcal{I}' = \mathbb{R}^{H' \times W' \times CH}$ , where  $H' > H$  and  $W' > W$ . Specifically, the panorama  $x' \in \mathcal{I}'$  is constructed by a series of spatial-ordered image crops  $\mathcal{X} = \{x_i \mid x_i \in \mathcal{I}, i = 1, 2, \dots, n\}$ , where each  $x_i$  represents an individual image segment.

Similar to language modeling, we define a joint probability distribution to learn how these crops interrelate to form a panorama  $x'$ :

$$\begin{aligned}
 P(x') &= P(x_1, x_2, \dots, x_n) \\
 &= \prod_{i=1}^n P(x_i \mid x_1, x_2, \dots, x_{i-1})
 \end{aligned} \tag{1}$$

where each  $P(x_i \mid x_1, x_2, \dots, x_{i-1})$  represents the condi-

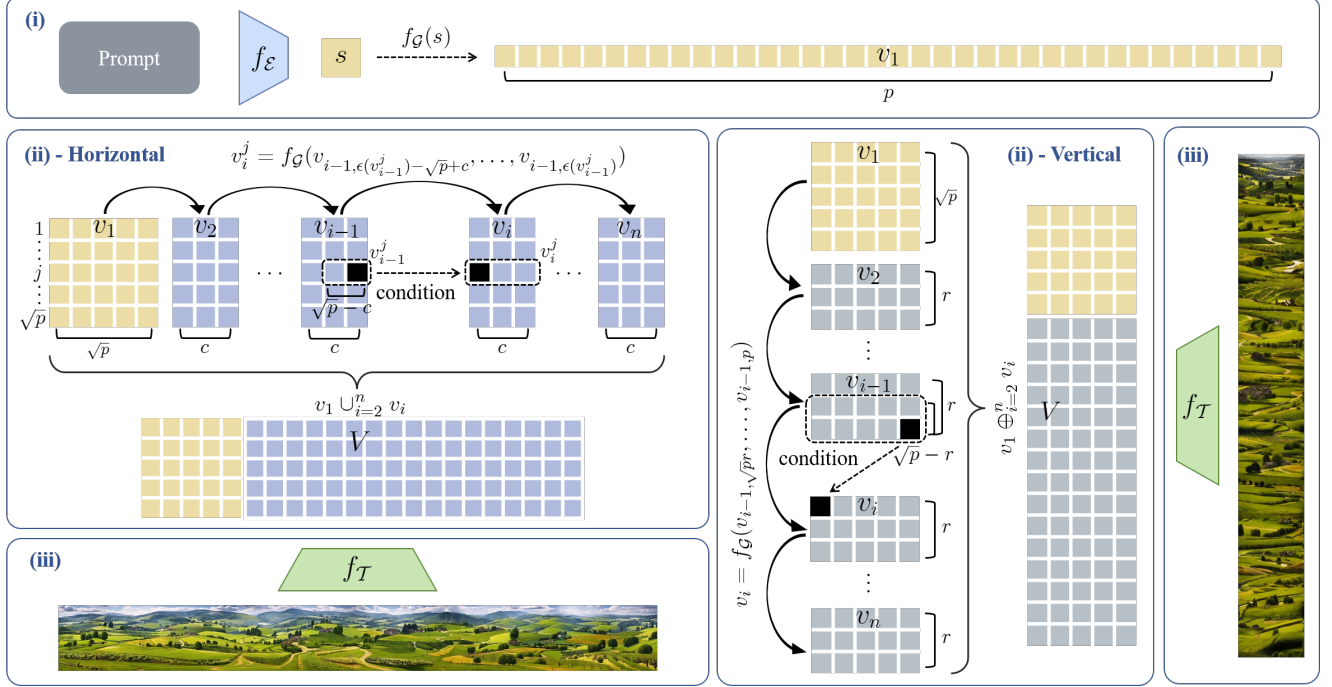


Figure 2. The framework of our PanoLlama can be divided into three parts: (i) **Textual Conditioning**: The given prompt  $y$  is encoded into a conditional embedding  $s$  using the text encoder  $f_{\mathcal{E}}$  (Eq. (6)). (ii) **Next-Crop Prediction**: With  $s$  as the initial input, the token generator  $f_{\mathcal{G}}$  generates a sequence of  $p$  tokens for the first crop  $v_1$  following an autoregressive next-token prediction approach (Eq. (7)). After reaching the token limit, **vertical expansion** is achieved by setting  $v_i$  to begin with the last  $p - \sqrt{p}r$  tokens of  $v_{i-1}$ , ensuring seamless continuity by Eq. (8). For **horizontal expansion**, we extend rows interleavingly by Eq. (10), letting the last  $\sqrt{p} - c$  tokens of each preceding row  $v_{i-1}^j$  serve as the start condition for  $v_i^j$ . (iii) **Decoding Tokens into Panorama**: After  $n$  rounds of expansion, the final concatenated token sequence  $V$  is decoded into the panoramic image  $x'$  by the image tokenizer decoder  $f_{\mathcal{T}}$  (Eq. (12)).

tional probability of generating the  $i$ -th image crop given the preceding tokens.

In panorama generation, the core is to achieve smooth transitions between each pair of neighboring crops  $x_{i-1}$  and  $x_i$ . Thus, we can adopt the Markov Chain assumption of order 1:

$$P(x_i | x_1, x_2, \dots, x_{i-1}) = P(x_i | x_{i-1}) \quad (2)$$

Under this assumption, Eq. (1) simplifies to:

$$P(x') = \prod_{i=2}^n P(x_i | x_{i-1}) \quad (3)$$

This formulation mirrors **next-token prediction** in language models but is applied to generating coherent adjacent image crops.

Taking the logarithm of both sides of Eq. (3), we obtain our loss function:

$$\mathcal{L}(\theta) = -\log P(x' | \theta) = -\sum_{i=2}^n \log P(x_i | x_{i-1}; \theta) \quad (4)$$

Formally, the optimization task is:

$$\begin{aligned} \theta^* &= \arg \min_{\theta} \mathcal{L}(\theta) \\ &= \arg \min_{\theta} -\sum_{i=2}^n \log P(x_i | x_{i-1}; \theta) \end{aligned} \quad (5)$$

By leveraging a well-trained autoregressive model, we can estimate the optimal parameters  $\theta^*$  that maximize the likelihood of the observed sequence  $x'$ , effectively capturing both the visual and semantic coherence of the panorama data.

### 3.2. Framework of PanoLlama

We utilize pre-trained models from LlamaGen [27], an effective AR-based architecture designed to generate images at  $512 \times 512$  with a maximum token limit of  $p = 1024$ . Specifically, our framework incorporates FLAN-T5 XL [8] as the text encoder, VQ-VAE [31] as the image tokenizer, and Llama [29] as the token generator to achieve text-guided panorama generation.

Firstly, the textual prompt  $y$  is encoded into a conditional

embedding  $s$  by applying the text encoder function  $f_{\mathcal{E}}$ :

$$s = f_{\mathcal{E}}(y) \quad (6)$$

where  $f_{\mathcal{E}} : \mathcal{Y} \rightarrow \mathbb{R}^d$  maps the prompt space  $\mathcal{Y}$  to the textual embedding space  $\mathbb{R}^d$ .

With  $s$  as a prefilling, the token generator  $f_{\mathcal{G}}$  initiates the generating process for the first image crop  $x_1$ , producing a sequence of  $p$  tokens:

$$v_1 = f_{\mathcal{G}}(s) = \{v_{1,k} \mid k = 1, 2, \dots, p\} \quad (7)$$

This generation follows the autoregressive paradigm, where each token  $v_{1,k}$  is produced conditionally based on its prefix.

The model’s property indicates that the arrangement of image tokens follows a raster scan order. Therefore, during panoramic extension, we consider each token sequence as a  $\sqrt{p} \times \sqrt{p}$  block, achieving **next-crop prediction** in a row-wise and training-free manner.

**Vertical Expansion** Upon reaching the token limit for the first crop, the position index  $k$  is reset from  $p$  to  $p'$  to commence a new round, extending  $r = \frac{p-p'}{\sqrt{p}}$  rows as  $v_2$ . To ensure continuity while fully utilizing the maximum  $p$ , we set  $v_2$  to begin with the condition of  $v_{1,\sqrt{pr}}, \dots, v_{1,p}$ , i.e., the subsequence comprising the last  $p'$  tokens of  $v_1$ , with the generation process advancing as:

$$v_2 = f_{\mathcal{G}}(v_{1,\sqrt{pr}}, \dots, v_{1,p}) = \{v_{2,k} \mid k = 1, 2, \dots, \sqrt{pr}\} \quad (8)$$

This process is iteratively applied for  $n$  times, resulting in a series of token sequences  $\mathcal{V} = \{v_i \mid i = 2, \dots, n\}$ , with each  $v_i$  corresponds to the image crop  $x_i$ . Then the entire panorama is constructed by:

$$\begin{aligned} V &= v_1 \oplus_{i=2}^n v_i \\ &= \{v_{1,k} \mid k = 1, 2, \dots, p\} \\ &\quad \oplus \{v_{i,k} \mid i = 2, \dots, n, k = 1, 2, \dots, \sqrt{pr}\} \end{aligned} \quad (9)$$

where  $\oplus$  refers to the vertical concatenation operator.

**Horizontal Expansion** To maintain the original token arrangement mode, we extend rows in an interleaving manner. Let  $v_i^j$  denote the  $j$ -th row in the  $i$ -th block,  $\epsilon(v_i^j)$  denote the index of the end token in  $v_i^j$ . In the horizontal case, each adjacent row  $v_{i-1}^j$  and  $v_i^j$  need to be connected with successive and cohesive conditions. Thus, we modify Eq. (8) to let the last  $\sqrt{p} - c$  tokens of each  $v_{i-1}^j$  serves as the start condition for  $v_i^j$ . In each iteration, the length of each row is extended by  $c$  columns:

$$\begin{aligned} v_i^j &= f_{\mathcal{G}}(v_{i-1,\epsilon(v_{i-1}^j)-\sqrt{p}+c}, \dots, v_{i-1,\epsilon(v_{i-1}^j)}) \\ &= \{v_{i,k} \mid j = 1, 2, \dots, \sqrt{p}, k = c(j-1) + 1, \dots, cj\} \end{aligned} \quad (10)$$

Accordingly, Eq. (9) should be modified as:

$$\begin{aligned} V &= v_1 \cup_{i=2}^n v_i \\ &= \{v_{1,k} \mid k = 1, 2, \dots, p\} \\ &\quad \cup \{v_{i,k} \mid i = 2, \dots, n, k = 1, 2, \dots, \sqrt{p}c\} \end{aligned} \quad (11)$$

and  $\cup$  corresponds to the horizontal concatenation operator.

After the expansion, we convert  $V$  into a panorama  $x'$  through the decoder of image tokenizer  $f_{\mathcal{T}}$ :

$$x' = f_{\mathcal{T}}(V) \quad (12)$$

Here,  $f_{\mathcal{T}} : \mathbb{T}^{\frac{H'}{16} \times \frac{W'}{16}} \rightarrow \mathbb{R}^{H' \times W' \times CH}$  maps tokens to the image pixel space, and  $\mathbb{T}$  denotes the discrete token set.

The entire process is recapped in Fig. 2 and Algorithm. 1.

---

#### Algorithm 1 PanoLlama Generation Process

---

**Input:**  $f_{\mathcal{E}}, f_{\mathcal{G}}, f_{\mathcal{T}}$  ▷ pre-trained models: text encoder, token generator, image tokenizer  
 $p$  ▷ max token limit of image tokenizer  
 $y$  ▷ textual prompt  
 $mode$  ▷ direction of expansion  
 $n$  ▷ expansion iterations  
 $r, c$  ▷ rows and columns expanded per iteration

**Output:**  $x'$  ▷ panorama

$s \leftarrow f_{\mathcal{E}}(y)$   
 $v_1 \leftarrow f_{\mathcal{G}}(s)$

**function** GENERATE\_TOKENS-VERTICAL( $v_{i-1}, r$ )  
 $v_i \leftarrow f_{\mathcal{G}}(v_{i-1,\sqrt{pr}}, \dots, v_{i-1,p})$   
**return**  $v_i$   
**end function**

**function** GENERATE\_TOKENS-HORIZONTAL( $v_{i-1}, c$ )  
**for**  $j = 1, 2, \dots, \sqrt{p}$  **do**  
 $v_i^j \leftarrow f_{\mathcal{G}}(v_{i-1,\epsilon(v_{i-1}^j)-\sqrt{p}+c}, \dots, v_{i-1,\epsilon(v_{i-1}^j)})$   
**end for**  
**return**  $v_i$   
**end function**

**if**  $mode == \text{'Vertical'}$  **then**  
**for**  $i = 2, 3, \dots, n$  **do**  
 $v_i \leftarrow \text{GENERATE\_TOKENS-VERTICAL}(v_{i-1}, r)$   
**end for**  
 $V \leftarrow v_1 \oplus_{i=2}^n v_i$

**else if**  $mode == \text{'Horizontal'}$  **then**  
**for**  $i = 2, 3, \dots, n$  **do**  
 $v_i \leftarrow \text{GENERATE\_TOKENS-HORIZONTAL}(v_{i-1}, c)$   
**end for**  
 $V \leftarrow v_1 \cup_{i=2}^n v_i$

**end if**  
 $x' \leftarrow f_{\mathcal{T}}(V)$   
**Return**  $x'$

---

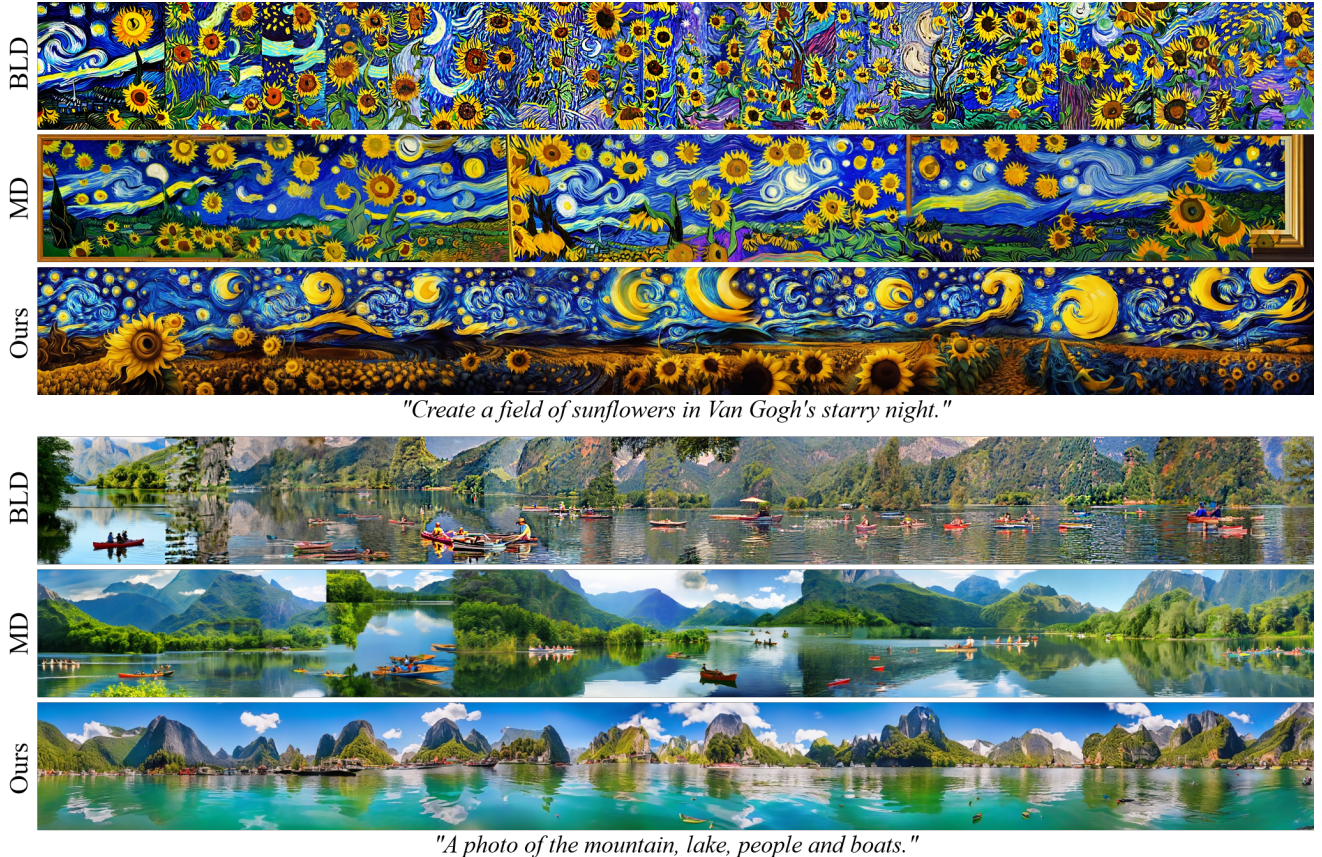


Figure 3. Qualitative comparisons between BLD, MD, and ours. Our approach effectively minimizes visible connections commonly found in diffusion-based methods, producing seamless  $512 \times 5120$  panoramas in both artwork (top) and real-scene (bottom) types.

### 3.3. Diffusion-Based Methods vs. PanoLlama

So far, the most effective approach for PIG tasks is joint diffusion [3, 15], which focuses on optimizing the connections between adjacent crops. According to our formulation in Sec. 3.1, we can view this paradigm from a new perspective, where its conditional dependency is expressed as  $P(x_i | x_{i-1}, x_{i+1})$ , indicating that the model generates each crop  $x_i$  by considering both features of its left and right neighbor. This leads to the joint probability:

$$P(x') = \prod_{i=1}^n P(x_i | x_{i-1}, x_{i+1}) \quad (13)$$

and similar to Eq. (4), the optimization objective can be defined as:

$$\begin{aligned} \mathcal{L}(\theta) &= -\log P(x' | \theta) \\ &= -\sum_{i=1}^n \log P(x_i | x_{i-1}, x_{i+1}; \theta) \end{aligned} \quad (14)$$

However, as discussed in Sec. 1 and Sec. 2, diffusion-based methods currently cannot achieve the optimal solu-

tion  $\theta^*$  for multilevel coherence. They intuitively divide the optimization goal into subtasks like controlling the connection process, enhancing spatial guidance, or deepening attention layers, each requiring a specialized technique. This lack of unity makes it difficult for them to achieve seamless transitions. In contrast, our approach leverages the autoregressive properties that inherently align with the PIG objective, forming a unified and stable framework that surpasses diffusion-based methods.

## 4. Experiments

### 4.1. Comparison

Our approach is evaluated and compared with multiple baselines in both qualitative and quantitative aspects.

**Implementation Details** To ensure the reliability of our results, we test 20 different prompts across 5 sets of random seeds, including various styles and content such as nature scenes (photorealistic), artworks (artistic), and semi-realistic scenarios (a blend of the two). For each prompt,

Table 1. Quantitative results comparing our PanoLlama with the baselines. Our method achieves the best overall performance across all the metrics, especially in coherence, aesthetics, and efficiency.

	Coherence		Fidelity & Diversity		Compatibility		Efficiency
	LPIPS↓	DISTS↓	FID↓	IS↑	CLIP↑	CLIP-aesthetic↑	time↓
SD	/	/	10.94	119.19	33.03	6.74	/
AR	/	/	9.36	80.27	31.56	6.75	/
MD	0.69	0.29	<u>12.55</u>	106.48	<b>33.26</b>	6.19	1802.48s
SyncD	<u>0.55</u>	<u>0.23</u>	16.76	<b>112.67</b>	<u>32.99</u>	6.39	1984.12s
MAD	0.69	0.31	13.54	100.35	31.43	6.22	2074.23s
BLD	0.83	0.47	89.08	86.54	32.30	5.76	2254.37s
SMD	0.73	0.30	25.86	90.52	30.80	5.53	<b>196.90s</b>
Ours	<b>0.41</b>	<b>0.19</b>	<b>12.10</b>	<u>111.63</u>	31.62	<b>6.85</b>	<u>723.01s</u>

we generate 100 panoramas at a resolution of  $512 \times 5120$ . Additionally, the results presented in Sec. 4.1 are generated with an expansion degree of  $c = 24$ , a transition factor of  $\lambda = 1.0$ , and the default parameter settings of the pre-trained models. More details and comparisons regarding these key factors are discussed in Sec. 4.2.

**Baselines** We compare our PanoLlama with five previous works: MultiDiffusion (MD) [3], SyncDiffusion (SyncD) [15], Merge-Attend-Diffuse (MAD) [19], Blended Latent Diffusion (BLD) [1], and StreamMultiDiffusion (SMD) [14]. The first three employ the joint diffusion pattern, while others are inpainting-based approaches. To ensure fairness, we standardize their expansion stride to 16. Moreover, we evaluate the pre-trained models used for panorama generation as benchmarks. For our AR-based method, we assess LlamaGen; for diffusion-based methods, we test two variants: the widely used Stable Diffusion (SD) v2.0 [21] and its advanced version, Stable Diffusion XL (SDXL) v1.0 [18], with further details provided in Appendix B.

**Evaluation Metrics** We apply a series of quantitative metrics to assess the following four aspects: (i) visual coherence at crop intersections, (ii) fidelity and diversity of generated panoramas, (iii) compatibility with textual inputs, (iv) efficiency of inference. To avoid feature loss and distortion caused by downscaling the entire panoramic image to fit the input requirements of certain metrics, we evaluate images cropped from panoramas at  $512 \times 512$ , a method that is widely adopted in related studies [3, 15, 39].

- **Coherence:** LPIPS [37] and DISTS [9] measure perceptual differences between image pairs. Each generated panorama is divided into 9 pairs of adjacent but non-overlapping crops. We randomly select 4,000 pairs for analysis.
- **Fidelity & Diversity:** FID [11] and IS [23] describe quality and variety of results by comparing the distributions of generated images with reference images. The former

are cropped images mentioned above. The latter are generated by pre-trained models, i.e., AR models for our PanoLlama and SD v2.0 for other baselines. To minimize the interference from coherence, we extract only 1 random crop from each panorama, 2,000 crops in total.

- **Compatibility:** CLIP [20] assesses cosine similarity between input prompts and generated images, while the CLIP-aesthetic score [24] is obtained from a linear model on CLIP. For each prompt, we use the aforementioned cropped images to calculate the scores.
- **Efficiency:** We measure the model’s runtime speed by the inference time taken to generate a batch of 50 panoramas on an A100 GPU.

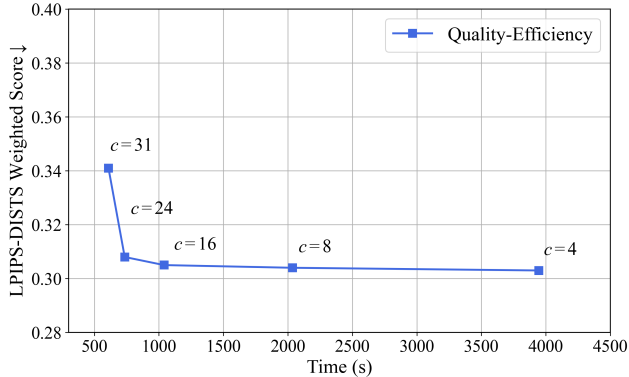
**Qualitative Results** As shown in Fig. 3, Blended Latent Diffusion displays artificial seams and repetitive segments during its extrapolation process. While MultiDiffusion improves on this, it still has unnatural junctions between image crops, particularly in artwork-type panoramas [39]. In contrast, our method consistently generates seamless panoramas, demonstrating significantly higher coherence even at lengths up to  $\times 10$  the original training resolution. More qualitative results are in Appendix A.

**Quantitative Results** Tab. 1 reports the mean scores of the metrics, with the best score in bold and the second-best underlined. Our PanoLlama outperforms other baselines in the following aspects: (i) Coherence, the most critical factor in panoramic images, is greatly improved by our method, with LPIPS and DISTS scores reduced by 40.21% and 37.36% respectively. (ii) An improvement in the CLIP-aesthetic metric is also observed, indicating that the enhancement in coherence contributes to a better aesthetic quality. (iii) In terms of efficiency, except for the real-time generation method SMD, our generation speed is nearly 3 times faster than typical PIG frameworks. (iv) For metrics where we didn’t reach top scores, such as IS and CLIP, the likely reason is our results are closely tied to the AR-based

generation benchmark. As shown in the first two rows of the table, this emerging approach underperforms diffusion models in certain aspects.

## 4.2. Ablation

As described in Sec. 3.2, we generate tokens for panoramas stepwise due to the constraint of  $p = 1024$ . Two factors that influence its performance are outlined below.



(a) The LPIPS-DISTS weighted score remains low across different  $c$  values, with the optimal quality-efficiency balance achieved at  $c = 24$ .



(b) Visual results confirm the quantitative assessment. As  $c$  increases, there is little noticeable loss in quality.

Figure 4. The impacts of the expansion degree on our next-crop prediction process. The quantitative and qualitative results demonstrate its robustness to  $c$ .

**Expansion Degree** Take horizontal PIG, each iteration expands the 2D token sequence by  $c \in [0, \sqrt{p}]$  columns, resulting in an overlapping region of  $\sqrt{p} - c$  columns between  $x_{i-1}$  and  $x_i$ . We investigate the impact of expansion degree on our next-crop prediction performance, testing  $c$  values of 4, 8, 16, 24, and 31. Since coherence is the key attribute for panoramas, we refine our evaluation by focusing on the LPIPS and DISTS metrics

As shown in Fig. 4a, the LPIPS-DISTS weighted score remains consistently low, exhibiting a slight rise when  $c$  reaches its upper limit 31. It indicates that our method is highly robust and insensitive to the change of expansion degree, with the best quality-efficiency trade-off achieved at  $c = 24$ . This finding is also supported by visual results presented in Fig. 4b.

**Transition factor** We can introduce a transition factor  $\lambda$  to perform linear interpolation between token embeddings, defined as:

$$\begin{aligned} \bar{e}_a &= \lambda e_a + (1 - \lambda) e_b \\ a^* &= \arg \min_a \|\bar{e}_a - e\|^2 \end{aligned} \quad (15)$$

where  $e$  represents the embedding weights of the pre-trained quantizer in  $f_{\mathcal{T}}$ ,  $e_a, e_b$  refer to the embeddings indexed by the corresponding tokens  $a, b$ , and  $a^*$  is the resulting token after the transition. Specially, when incorporating Eq. (15) into the expansion process described in Eq. (8) and Eq. (10), the tokens  $a$  and  $b$  correspond to the adjacent tokens at the boundary between  $v_{i-1}$  and  $v_i$ .

To evaluate whether embedding interpolation leads to smoother transitions in panorama content, we analyze the aforementioned LPIPS-DISTS weighted score for different  $\lambda$  values from 0 to 1, sampling 100 points for the test. As seen in Fig. 5, the performance of our PanoLlama peaks at  $\lambda = 1.0$ , with a decline at other values. This suggests our method reaches its best without the need for embedding transitions.

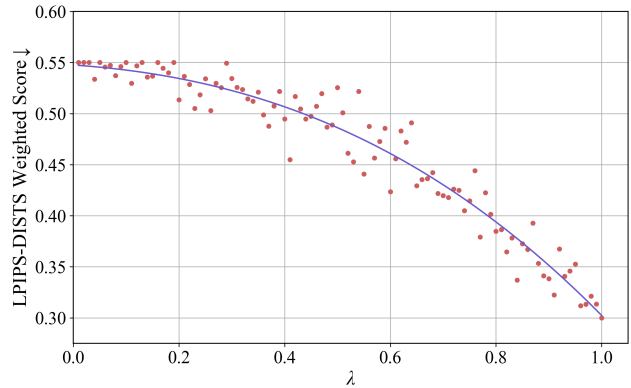


Figure 5. Ablation study about the transition factor in Eq. (15). The model performed best at  $\lambda = 1$ , meaning that our method works well without embedding interpolation.

## 4.3. Applications

In addition to text-to-panorama generation, we offer a range of applications that leverage our framework’s capabilities.



Figure 6. Versatile applications of our PanoLlama, including multi-scale, multi-layout, and multi-guidance generation.

**Multi-Scale** We support expansion in horizontal, vertical, and both directions. Note that in the third case, vertical expansion should be prioritized to achieve the desired image height, followed by horizontal expansion to extend the width. This yields better results than applying horizontal expansion first. Fig. 6 (i) displays the multi-scale results, with sizes of  $3072 \times 512$  and  $3072 \times 3072$  respectively.

**Multi-Layout** Our method allows for flexible adjustments in rows  $r$ , columns  $c$ , and prompts  $y$ , enabling layout-based generation controlled by users. Employing Eq. (15) with  $0.5 < \lambda < 0.8$ , we achieve smooth transitions in token embeddings across different textual conditions. As shown in Fig. 6 (ii), we assign different prompts to different regions (top), and our PanoLlama effectively blends them into a storytelling panorama that is visually and semantically coherent (bottom).

**Multi-Guidance** Beyond text-guided generation, our framework also accommodates image guidance and mixed guidance. Input images are tokenized by the encoder of the pre-trained  $f_{\mathcal{T}}$ , which then serves as the condition for generation. Fig. 6 (iii) illustrates two examples where the text

and image collaboratively guide the generation process, resulting in an effect similar to image inpainting.

## 5. Conclusion

Coherence is one of the major pending challenges in panoramic image generation. In this paper, we introduce PanoLlama as a novel solution, framing panorama generation as a next-token prediction task. This approach has several key advantages over the existing methods: (i) We redefine a more reasonable paradigm for PIG tasks, fundamentally demonstrating our superiority over diffusion-based methods. (ii) We developed a training-free AR-based strategy, achieving panorama generation of high quality and arbitrary size. (iii) PanoLlama is a unified, robust, and versatile framework that can be applied to multiple tasks beyond text-to-panorama generation.

**Limitations** Our method imposes no constraints on subject layout, which may lead to a panorama lacking a clear focal point, as each crop presents similar content. Additionally, our method’s performance heavily relies on pre-trained AR models, which are currently not as well-established as SD models.



## Acknowledgements

We thank Yunhao Chen for his key contributions to this study, including the idea development and core method code.

## References

- [1] Omri Avrahami, Ohad Fried, and Dani Lischinski. Blended latent diffusion. *ACM Transactions on Graphics (TOG)*, 42(4):1–11, 2023. [2](#), [6](#)
- [2] Yutong Bai, Xinyang Geng, Karttikeya Mangalam, Amir Bar, Alan L Yuille, Trevor Darrell, Jitendra Malik, and Alexei A Efros. Sequential modeling enables scalable learning for large vision models. In *Proceedings of the IEEE/CVF Conference on Computer Vision and Pattern Recognition*, pages 22861–22872, 2024. [1](#)
- [3] Omer Bar-Tal, Lior Yariv, Yaron Lipman, and Tali Dekel. Multidiffusion: Fusing diffusion paths for controlled image generation. In *International Conference on Machine Learning*, pages 1737–1752, 2023. [1](#), [2](#), [5](#), [6](#)
- [4] Tom B. Brown, Benjamin Mann, Nick Ryder, Melanie Subbiah, Jared Kaplan, Prafulla Dhariwal, Arvind Neelakantan, Pranav Shyam, Girish Sastry, Amanda Askell, et al. Language models are few-shot learners. In *Advances in Neural Information Processing Systems*, pages 1877–1901, 2020. [2](#)
- [5] Shiyue Cao, Yueqin Yin, Lianghua Huang, Yu Liu, Xin Zhao, Deli Zhao, and Kaigi Huang. Efficient-vqgan: Towards high-resolution image generation with efficient vision transformers. In *Proceedings of the IEEE/CVF International Conference on Computer Vision*, pages 7368–7377, 2023. [2](#)
- [6] Huiwen Chang, Han Zhang, Lu Jiang, Ce Liu, and William T Freeman. Maskgit: Masked generative image transformer. In *Proceedings of the IEEE/CVF Conference on Computer Vision and Pattern Recognition*, pages 11315–11325, 2022. [2](#)
- [7] Yunhao Chen, Zihui Yan, and Yunjie Zhu. A comprehensive survey for generative data augmentation. *Neurocomputing*, page 128167, 2024. [1](#)
- [8] Hyung Won Chung, Le Hou, Shayne Longpre, Barret Zoph, Yi Tay, William Fedus, Yunxuan Li, Xuezhi Wang, Mostafa Dehghani, Siddhartha Brahma, et al. Scaling instruction-finetuned language models. *Journal of Machine Learning Research*, 25(70):1–53, 2024. [3](#)
- [9] Keyan Ding, Kede Ma, Shiqi Wang, and Eero P Simoncelli. Image quality assessment: Unifying structure and texture similarity. *IEEE transactions on pattern analysis and machine intelligence*, 44(5):2567–2581, 2020. [6](#)
- [10] Patrick Esser, Robin Rombach, and Bjorn Ommer. Taming transformers for high-resolution image synthesis. In *Proceedings of the IEEE/CVF conference on computer vision and pattern recognition*, pages 12873–12883, 2021. [2](#)
- [11] Martin Heusel, Hubert Ramsauer, Thomas Unterthiner, Bernhard Nessler, and Sepp Hochreiter. Gans trained by a two time-scale update rule converge to a local nash equilibrium. *Advances in neural information processing systems*, 30, 2017. [6](#)
- [12] Jonathan Ho, Ajay Jain, and Pieter Abbeel. Denoising diffusion probabilistic models. *Advances in neural information processing systems*, 33:6840–6851, 2020. [1](#)
- [13] Rui Jiang, Guang-Cong Zheng, Teng Li, Tian-Rui Yang, Jing-Dong Wang, and Xi Li. A survey of multimodal controllable diffusion models. *Journal of Computer Science and Technology*, 39(3):509–541, 2024. [1](#)
- [14] Jaerin Lee, Daniel Sungho Jung, Kanggeon Lee, and Kyoung Mu Lee. Streammultidiffusion: Real-time interactive generation with region-based semantic control. *arXiv preprint arXiv:2403.09055*, 2024. [2](#), [6](#)
- [15] Yuseung Lee, Kunho Kim, Hyunjin Kim, and Minhyuk Sung. Syncdiffusion: Coherent montage via synchronized joint diffusions. *Advances in Neural Information Processing Systems*, 36:50648–50660, 2023. [1](#), [2](#), [5](#), [6](#)
- [16] Jialu Li and Mohit Bansal. Panogen: Text-conditioned panoramic environment generation for vision-and-language navigation. *Advances in Neural Information Processing Systems*, 36, 2024. [2](#)
- [17] Xiang Li, Kai Qiu, Hao Chen, Jason Kuen, Zhe Lin, Rita Singh, and Bhiksha Raj. Controlvar: Exploring controllable visual autoregressive modeling. *arXiv preprint arXiv:2406.09750*, 2024. [2](#)
- [18] Dustin Podell, Zion English, Kyle Lacey, Andreas Blattmann, Tim Dockhorn, Jonas Müller, Joe Penna, and Robin Rombach. SDXL: Improving latent diffusion models for high-resolution image synthesis. In *The Twelfth International Conference on Learning Representations*, 2024. [6](#)
- [19] Fabio Quattrini, Vittorio Pippi, Silvia Cascianelli, and Rita Cucchiara. Merging and splitting diffusion paths for semantically coherent panoramas. *arXiv preprint arXiv:2408.15660*, 2024. [1](#), [2](#), [6](#)
- [20] Alec Radford, Jong Wook Kim, Chris Hallacy, Aditya Ramesh, Gabriel Goh, Sandhini Agarwal, Girish Sastry, Amanda Askell, Pamela Mishkin, Jack Clark, et al. Learning transferable visual models from natural language supervision. In *International conference on machine learning*, pages 8748–8763, 2021. [6](#)
- [21] Robin Rombach, Andreas Blattmann, Dominik Lorenz, Patrick Esser, and Björn Ommer. High-resolution image synthesis with latent diffusion models. In *Proceedings of the IEEE/CVF conference on computer vision and pattern recognition*, pages 10684–10695, 2022. [1](#), [6](#)
- [22] Ludan Ruan, Yiyang Ma, Huan Yang, Huiguo He, Bei Liu, Jianlong Fu, Nicholas Jing Yuan, Qin Jin, and Baining Guo. Mm-diffusion: Learning multi-modal diffusion models for joint audio and video generation. In *Proceedings of the IEEE/CVF Conference on Computer Vision and Pattern Recognition*, pages 10219–10228, 2023. [1](#)
- [23] Tim Salimans, Ian Goodfellow, Wojciech Zaremba, Vicki Cheung, Alec Radford, and Xi Chen. Improved techniques for training gans. *Advances in neural information processing systems*, 29, 2016. [6](#)
- [24] Christoph Schuhmann, Romain Beaumont, Richard Vencu, Cade Gordon, Ross Wightman, Mehdi Cherti, Theo Coombes, Aarush Katta, Clayton Mullis, Mitchell Wortsman, et al. Laion-5b: An open large-scale dataset for training

- next generation image-text models. *Advances in Neural Information Processing Systems*, 35:25278–25294, 2022. 6
- [25] Jascha Sohl-Dickstein, Eric Weiss, Niru Maheswaranathan, and Surya Ganguli. Deep unsupervised learning using nonequilibrium thermodynamics. In *International conference on machine learning*, pages 2256–2265, 2015. 1
- [26] Jiaming Song, Chenlin Meng, and Stefano Ermon. Denoising diffusion implicit models. In *International Conference on Learning Representations*, 2021. 1
- [27] Peize Sun, Yi Jiang, Shoufa Chen, Shilong Zhang, Bingyue Peng, Ping Luo, and Zehuan Yuan. Autoregressive model beats diffusion: Llama for scalable image generation. *arXiv preprint arXiv:2406.06525*, 2024. 1, 2, 3
- [28] Keyu Tian, Yi Jiang, Zehuan Yuan, Bingyue Peng, and Liwei Wang. Visual autoregressive modeling: Scalable image generation via next-scale prediction. *arXiv preprint arXiv:2404.02905*, 2024. 2
- [29] Hugo Touvron, Thibaut Lavril, Gautier Izacard, Xavier Martinet, Marie-Anne Lachaux, Timothée Lacroix, Baptiste Rozière, Naman Goyal, Eric Hambro, Faisal Azhar, et al. Llama: Open and efficient foundation language models. *arXiv preprint arXiv:2302.13971*, 2023. 2, 3
- [30] Aäron Van Den Oord, Nal Kalchbrenner, and Koray Kavukcuoglu. Pixel recurrent neural networks. In *International conference on machine learning*, pages 1747–1756, 2016. 2
- [31] Aaron Van Den Oord, Oriol Vinyals, et al. Neural discrete representation learning. *Advances in neural information processing systems*, 30, 2017. 2, 3
- [32] Jionghao Wang, Ziyu Chen, Jun Ling, Rong Xie, and Li Song. 360-degree panorama generation from few unregistered nfov images. In *Proceedings of the 31st ACM International Conference on Multimedia*, pages 6811–6821, 2023. 2
- [33] Xinlong Wang, Xiaosong Zhang, Zhengxiong Luo, Quan Sun, Yufeng Cui, Jinsheng Wang, Fan Zhang, Yueze Wang, Zhen Li, Qiyang Yu, et al. Emu3: Next-token prediction is all you need. *arXiv preprint arXiv:2409.18869*, 2024. 2
- [34] Tianhao Wu, Chuanxia Zheng, and Tat-Jen Cham. Panodiffusion: 360-degree panorama outpainting via diffusion. In *The Twelfth International Conference on Learning Representations*, 2024. 2
- [35] Hang Yu, Ruilin Li, Shaorong Xie, and Jiayan Qiu. Shadow-enlightened image outpainting. In *Proceedings of the IEEE/CVF Conference on Computer Vision and Pattern Recognition*, pages 7850–7860, 2024. 2
- [36] Lijun Yu, Jose Lezama, Nitesh Bharadwaj Gundavarapu, Luca Versari, Kihyuk Sohn, David Minnen, Yong Cheng, Agrim Gupta, Xiuye Gu, Alexander G Hauptmann, Boqing Gong, Ming-Hsuan Yang, Irfan Essa, David A Ross, and Lu Jiang. Language model beats diffusion - tokenizer is key to visual generation. In *The Twelfth International Conference on Learning Representations*, 2024. 1, 2
- [37] Richard Zhang, Phillip Isola, Alexei A Efros, Eli Shechtman, and Oliver Wang. The unreasonable effectiveness of deep features as a perceptual metric. In *Proceedings of the IEEE conference on computer vision and pattern recognition*, pages 586–595, 2018. 6
- [38] Xiaoyu Zhang, Teng Zhou, Xinlong Zhang, Jia Wei, and Yongchuan Tang. Multi-scale diffusion: Enhancing spatial layout in high-resolution panoramic image generation. *arXiv preprint arXiv:2410.18830*, 2024. 1, 2
- [39] Teng Zhou and Yongchuan Tang. Twindiffusion: Enhancing coherence and efficiency in panoramic image generation with diffusion models. In *ECAI 2024*, pages 386–393. IOS Press, 2024. 2, 6

## A. More Qualitative Comparison Results

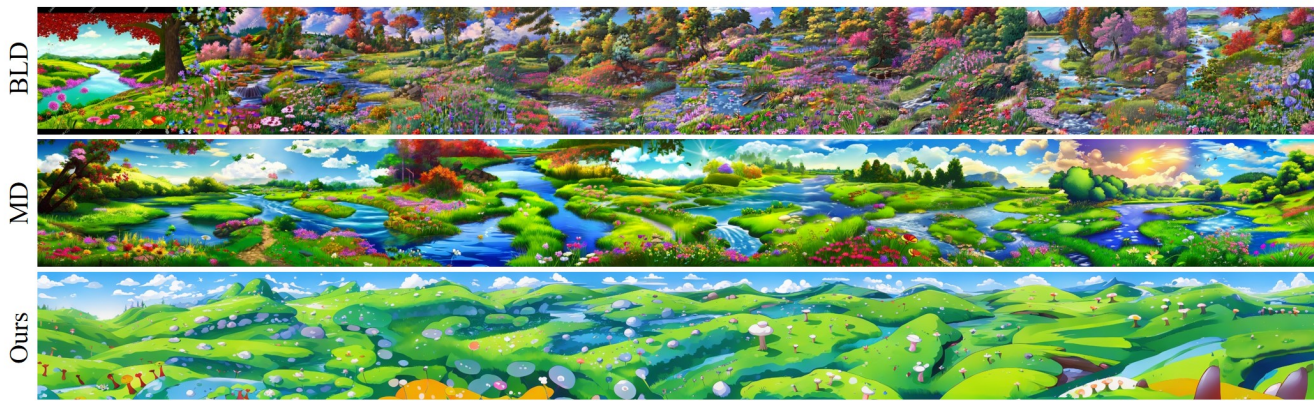
Figs. A1 to A5 gives more qualitative comparisons on panoramic image generation ( $512 \times 5120$ ), highlighting the areas where improvements have been made.



Figure A1. Additional qualitative comparison results on panorama generation with various text prompts.



*"An oil painting of red and yellow flowers blooming lively."*



*"Natural landscape in anime style with green meadows, streams, wildflowers and mushrooms."*



*"A hand-embroidered design of antique floral patterns."*

Figure A2. Additional qualitative comparison results on panorama generation with various text prompts.



*"A rock concert with crowd and colorful stage lights."*



*"Cityscape at a clear night illuminated by neon lights."*



*"A mosaic style artwork of a collage with the designs of Gaudi."*

Figure A3. Additional qualitative comparison results on panorama generation with various text prompts.



*"A digital painting of planets in dreamy universe."*



*"A paper-cut style portrayal of a traditional Chinese festival celebration."*



*"Create a world of a coastline with various corals and fishes."*

Figure A4. Additional qualitative comparison results on panorama generation with various text prompts.



*"A cyaneous night sky filled with stars shining and scattering around, illuminating a vast desert landscape."*



*"A landscape ink painting."*



*"Generate a sprawling, verdant countryside."*

Figure A5. Additional qualitative comparison results on panorama generation with various text prompts.

## B. Comparison with the Advanced Diffusion Models

We also conduct experiments using advanced diffusion models as comparison baselines, replacing the pre-trained models in baselines from SD v2.0 with SDXL v1.0. Considering that images generated by SDXL have larger dimensions of  $1024 \times 1024$ , we generate images of  $1024 \times 5120$  and still crop them to  $512 \times 512$  to align with the other image sets.

Tab. A1 presents the comparison results. Notably, even with SDXL, our approach excels at enhancing the visual and semantic coherence of generated panoramas, though to a lesser degree than the SD-based reference model. This is expected, given SDXL’s advanced design as a diffusion model with doubled default resolution in both height and width.

Table A1. Comparisons among SD-based methods using advanced diffusion models. Our approach still stands out in improving the coherence of the generated panoramas while maintaining aesthetic quality and operational speed.

	Coherence		Fidelity & Diversity		Compatibility		Efficiency
	LPIPS ↓	DISTS ↓	FID ↓	IS ↑	CLIP ↑	CLIP-aesthetic ↑	time ↓
SD <sub>XL</sub>	/	/	8.24	124.80	33.12	6.80	/
AR	/	/	9.36	80.27	31.56	6.75	/
MD <sub>XL</sub>	0.54	0.23	12.30	110.43	33.43	6.26	5697.99s
SyncD <sub>XL</sub>	0.45	0.21	13.11	<b>119.77</b>	<b>33.50</b>	6.45	7868.80s
MAD <sub>XL</sub>	0.56	0.29	13.01	100.94	31.19	6.23	6513.78s
BLD <sub>XL</sub>	0.80	0.44	85.83	90.23	32.15	5.78	6981.89s
SMD <sub>XL</sub>	0.62	0.30	20.55	96.37	31.49	5.53	<b>513.31s</b>
Ours	<b>0.41</b>	<b>0.19</b>	<b>12.20</b>	108.82	31.19	<b>6.85</b>	1449.32s